CHARACTERIZATION OF COLLAGEN FIBRIL DIAMETER DISTRIBUTION AND BIOMECHANICAL PROPERTIES OF HEALTHY AND INJURED RAT ANTERIOR CRUCIATE LIGAMENT

Adeoye Abass Ojo, Bachelor of Science

Submitted in fulfillment of the requirements for the degree of a Master of Science in Biomedical Engineering

School of Engineering and Digital Sciences
Department of Chemical and Materials Engineering
Nazarbayev University

53 Kabanbay Batyr Avenue,
Nur-Sultan, Kazakhstan, 010000

Supervisors:

Lead Supervisor Name: Associate Professor Cevat Erisken

Co-supervisor Name: Associate Professor Enrico Marsili

April 2022

Declaration

I hereby declare that this manuscript, entitled "Characterization of collagen fibril diameter distribution and biomechanical properties of healthy and injured rat Anterior Cruciate Ligament" is the result of my work except for quotations and citations which have been duly acknowledged.

I also declare that, to the best of my knowledge and belief, it has not been previously or concurrently submitted, in whole or in part, for any other degree or diploma at Nazarbayev University or any other national or international institution.

Name: Adeoye Abass Ojo

Date: 04.04.2022

Acknowledgements

I would like to express my gratitude to all of the individuals who made such a significant contribution to thesuccessful completion of this research project. First and foremost, I would like to express my profound gratitudeto my supervisor, Prof. Cevat Erisken, for his patience and support, as well as for his insightful and helpful ideas throughout the design, execution, development, and writing of this research project. I would like to express my gratitude to Prof. Enrico Marsili, my co-supervisor, for his assistance. I also want to express my gratitude to Sanazar Kadyr, Leya Timur, Ulpan Nurmanova, Banu Seitzhaparova, Baisunkar Mirasbek, Bakhytbol Khumyrzakh, Aida Zhakypbekova my BIREL laboratory colleagues, for their support and assistance with the experiments. Their words of support, evaluation and comments have all contributed significantly to the success of this project. I will also want to thank Nurgul Daniyeva and Laura Khamkhash, Nazarbayev University Research Technologists, for their invaluable advice and assistance with specimen preparation and imaging with TEM and SEM. I also express my gratitude to Micheal Shola-David, Isiaq Sanusi, and Andrew Demba, my brothers from my homeland, for their support.

Last but not least, I want to express my gratitude to my parents, Mr., and Mrs. Adeoye, as well as my brothersand cousins. Without their love, encouragement, and all-around support, none of this would have been possible.

Table of Contents

List of abbreviations

ACL	Anterior Cruciate Ligament
AT	Achilles Tendon
DCM	Dichloromethane
DDSA	Dodecenylsuccinic anhydride
ECM	Extracellular matrix
FT	Flexor Tendon
MCL	Medial Collateral Ligament
MNA	Methyl nadic anhydride
PCL	Polycaprolactone
PBS	Phosphate buffer solution
PT	Patellar Tendon
SEM	Scanning Electron Microscopy
TEM	Transmission Electron Microscopy
ANOVA	Analysis of Variance
AA	Acetic Acid

List of Figures and Tables

Abstract

With frequent leaping, colliding, turning, and cutting, women and men involved in sports-related activities are more vulnerable to anterior cruciate ligament (ACL) ruptures compared to the rest of the population. Researchers have shown that kinematics and neuromuscular control of the knee joint are affected inversely following ACL damage. Reconstructed ACLs cannot completely restore these adaptations, and it is critical to provide a physiologically viable environment for optimal biomaterial-cell interaction. Since ACL reconstruction procedures frequently result in failure or inferior scar tissue is formed, new strategies are needed to regenerate the torn/ruptured ACL tissue. In animal models of bovine and sheep, the ACL injuries were previously shown to lead to a change in the distribution of collagen fibrils diameter, with a shift from a bimodal distribution in the healthy ACL to a unimodal distribution after injury.

In this study, it is hypothesized that the collagen fibril diameter distribution in rat ACL changes from a bimodal distribution in the healthy ACLto a unimodal distribution after injury and that this change can be mimicked in scaffolds fabricated using electrospinning. This hypothesis was tested by first creating an injured rat ACL model by applying a mechanical tensile force to the healthy ACL tissue until rupture. Secondly, transmission electron microscopy(TEM) evaluation of the healthy and injured ACL tissues was carried out to evaluate the collagen fibril diameter distributions in the tissues. Thirdly, using the electrospinning approach, polycaprolactone (PCL) scaffolds were created to imitate the bimodal and unimodal distributions of collagen fibrils seen in healthy and injured tissues, respectively. The mechanical properties of ACL and PCL electrospun nanofiber scaffolds were also tested at a crosshead speed of 5 mm/min under tension.

Findings reveal that the bimodal distribution of ACL collagen fibril diameter changed to unimodal after injury, causing a decrease in the mean diameter. In healthy ACL, the fiber diameter distribution

of PCL electrospun scaffolds were qualitatively and quantitatively similar. Native ACL tissue outperformed PCL scaffolds biomechanically. This study is significant because it addresses a major clinical issue that affects millions of people globally. The suggested bimodal fibrous scaffold design deviates from the usual unimodal scaffolds and may have a significant influence on the behavior of ACL cells and thus on ACL regeneration.

Keywords: Ligament, Kinematics, Neuromuscular, integration, ACL, PCL, Transmission Electron Microscope, Polycaprolactone, Electrospun, Nanofiber, scaffolds.

CHAPTER 1- (INTRODUCTION)

1.1 Anterior Cruciate Ligament

Ligaments connect bones to bones. The ACL in the knee joint, which acts as a resistor and stabilizerfor anterior tibial and rotational stresses, is one of the most important components in the knee joint[1]. It is essential for knee joint stability and kinematics[2]. When the knee is stretched, the posterolateral bundle will get tight and the anteromedial bundle will relax depending on the viscoelastic and biomechanical properties of the ACL, which are controlled mainly by the collagen fibrils [3].

1.1.1 ACL Composition and Structure

The ACL is a weakly vascularized connective tissue that is mostly made up of well-alignedtype 1 collagen fibrils and surrounded by connective tissue cells i.e., fibroblasts, elastin, and glycoproteins as well as glycosaminoglycans. The ACL serves as a connector between the femur and the tibia with the major role of knee stabilizer by serving as the resistor that translates anteriortibial and rotational loads[1]. Human ACL is reported to be irregular in geometry and it has an areaof approximately $34mm^2$ and $42mm^2$ both at the femur and the tibial junctions, respectively. ACLis made up of fascicles that comprise fibrils and fibroblasts. Fibroblasts are connective tissue cells that secrete components of the matrix and make up of approximately one-fifth of the entire volume of the tissue, the remaining part being the extracellular matrix[4].

1.1.2 Function of Anterior Cruciate Ligament

The complete kinematics regarding the back-and-forth movement of the knee is being controlled by the ACL. The ACL is positioned diagonally at the center of the knee (Figure 1). It prevents the tibia from skidding out of the femur and provides stability of rotation to the knee[5]. The role of the ACL in the stability of the knee joint is very important and a slight tear or rupture of the ACL leads to its instability, which is, then, followed by tears to the meniscus as well as initiation of osteoarthritis[6].

1.1.3 Biomechanical properties of ACL

Because the mechanical attributes of the ACL are so intimately linked to the structure of collagen fibrils, a variation in the distribution of collagen fibrils in the ACL can result in a reduction in mechanical resistance to force, which can lead to tears and rupture. In this perspective, collagen diameter and volume are important ACL features since they ultimately determine the tissue's tensile strength and stability[7]. According to prior research examining the relationship between mechanical properties and fibril diameter[4], a physiological range of fibril diameter is essential for optimal ACL function. Under tensile loading, the stress-strain behavior ofACL exhibits a tri-phasic pattern that includes the toe, linear, and yield zones[8]. The pattern in the fibrils in the toe region straightens out at low stresses, requiring lower pressures. In the linear area, at the beginning of elastic deformation, the resistance pressure steadily increases. The yield area signifies the beginning of irreversible deformation, and due to the tearing of collagen fibrils at this point, stress diminishes, resulting in the rupture of the ligament[8].

1.1.4 Clinical Problem and Treatment of ACL Injuries

Injuries due to ACL rupture are reported to occur more than 200,000 times every year in the United States [9]. Because of its hypocellular and minimally vascularized nature, and the frequency of motion, ACL injuries do not regenerate, and their healing process results in the development of a scar tissue. The ACL is frequently injured in sports as a result of axial loading coupled with the rotation of the valgus-internal angulation of the knee[10], and currently available medical treatments, i.e., reconstruction procedures, involving grafts of different sources are unable to effectively heal the ACL injuries[11]. Injury to the ACL is instantly problematic due to the functional imbalance, and it can lead to long-term complications such as injuries to the meniscus, secondary stabilizers failure, and the beginning of osteoarthritis early in life[12].

1.1.5 Rat Anterior Cruciate Ligament

Rat ACLs, like human ACLs, provide stability during joint movement. It is more prone to acute and chronic injury than other ligaments. Due to anatomical similarities between rats and human [13], this study employed rats as animal models to investigate the effect of injuryon the diameter of collagen fibrils in the ACL.

1.2 Ligament Tissue Engineering

Tissue engineering is an multidisciplinary field aiming at restoring the functions of tissues using biomaterials in addition to cells and biological factors. In order to design and fabricate a biomaterial scaffold for ligament repair and regeneration, the properties of ligaments need to be investigated. These properties differ depending on the anatomical location, age, and a variety of other variables connected with an injury or disease. The distinctive helical structuring of collagen fiber bundles is

considered to be important for the ligament to execute its stabilizing role on a structure-function level. When the human knee is rotated (140 degrees – in extension/flexion), the mechanism of attachment causes the ACL and peripheral fiber bundles to twist 90 degrees[14]. Therefore, in designing a scaffold for tissue engineering purposes, this hierarchical structure of the ligament andthe collagens should be considered and mimicked[15]. A 3D environmentmade up of porous scaffold is required to engineer a tissue. Cells and growth factors arealso required. The scaffold forms an ideal environment for cell multiplication, while growth factorsaid in the formation of new tissue [16]. Tissue engineering is a technique for repairing or replacingdamaged organs and tissues by infusing cells, scaffolds, proteins, DNA, and/or protein fragments during surgical procedures[17], [18].

1.2.1 Nanofiber Scaffolds

Artificial extracellular matrices known as nanofibrous scaffold offers a natural environmentfor tissue development. Because of their high surface over volume ratio, nanofibers have broadened the possibilities for constructing scaffolds mimicking the structure of natural human tissue at the nanoscale scale[19]. Because of their architectural similarities to the extracellular matrix, as well as their adaptable chemical and physical properties for influencing cell response and behavior, electrospun nanofibers have been widely preferred in regenerative engineering[20]. Thus, scaffolds with a 3D environment and biomimetic fibrous structures may offer stem cells a 3D micro/nano-habitats and biomimetic environment[21].

1.2.2 Growth Factors

Growth factors are naturally occurring chemical/biological substances that can promote cell behavior, wound repair, and tissue regeneration. It is usually a released protein and plays an essential role in a

variety of cellular activities. Growth factors make up proteins that have been found in the early stages of ligament development and are thought to play a key function in the healing process. These proteins induce cells to proliferate, produce and remodel the extracellular matrix [22]. Various cytokines also exhibit the ability to alter the cell behavior of ACL[17], [23].

1.2.3 Electrospinning for Nanofibers

The electrospinning technology has been proven to be capable of creating fibers on the nanometer scale[24]. Furthermore, electrospinning is a method that uses a high-voltage electric field to form electrically charged jets from a polymer solution, which are subsequently dried by evaporating the solvent to create solid nanofibers. The electrically charged fibers are directed straight into an oppositely charged collector, which can be a stationary surface or a spinning drum[24]. Additionally, during electrospinning, the jet is significantly extended owing to the acceleration in the direction of the counter electrode, and electrostatic forces overcome a surface tension when the voltage exceeds a threshold value, resulting in the release of a fine electrified jet[25]. Polymer solutions are utilized to produce diameters during electrospinning of fibers ranging from two nanometers to several micrometers[25], [26].

In a traditional electrospinning technique, electrostatic forces remove fibers from a solution through a blunt needle. Mats with randomly oriented or parallel-aligned strands are one alternative for collecting electrospun nanofibers[25]. Electrospun fiber characteristics are influenced by a variety of parameters, including polymer concentration (or viscosity), polymer solution feed rate, applied voltage, and distance [25]. Polymer concentration is known as one of the most influential parameters to control the diameter of electrospun fibers [27]. An optimum concentration is desirable to successfully spin the polymer solutions to form fibers in a desired range [28]. According to Bhardwaj et al 2010 and Weimin Yang 2019, for example, these parameters can be tailored to form fibers ranging between100-

1000nm[29]. In addition, the viscosity of the solution and the rate of solvent evaporation controlled by ambient temperature and humidity, can also affect diameter, surface pore characteristics, and spinnability of fibers [26], [28].

1.2.4 Mechanical Testing

The compressive, tensile, bending, and shear characteristics of tissue may be determined using mechanical testing procedures. Since the ACL, in its anatomic location, is frequently exposedto extensional type of forces, an appropriate test to determine its biomechanical properties should also be performed under tension. Uniaxial tensile procedures, in which an appropriately harvestedtissue is attached to the grips and stretched in opposite directions, are the most widely employed tests for investigating mechanical properties of the ACL [30]. Such tests can provide important tissue specific parameters such as ultimate stress, elastic modulus, and ultimate strain. The tensile testingregimes may be affected by the deformation, as well as the rate of each of these parameters[30]. The stress-strain curve for many soft tissues undergoes a non-linear transition as strain is increased, with uncrimped collagen becoming the dominant load-bearing constituent[31].

1.3. Framework of the Study

The collagen fibril diameter distribution of ACL was previously studied for bovine [32] and sheep [33] in our group, and it was found that the distribution changes from bimodal to unimodal upon injury. In order to generate a pool of data for other species for the generalizability of this behavior, this study aims at testing the hypothesis that the collagen fibril diameter distribution in rat ACL tissue will change from bimodal to unimodal upon injury. Specific aims are to i) investigate the collagen fibril diameter distribution of healthy and injured rat ACL tissue, ii) fabricate nanofiber scaffolds to

replicate the collagen fibril diameter distributions, and iii) compare the mechanical properties of native ACL tissue and nanofiber scaffolds.

Chapter 2 provides the materials and methods utilized to perform experiments for the stated specific aims, and the findings from these experiments are given in Chapter 3. Results are discussed in Chapter 4 and significant conclusions are given in Chapter 5.

CHAPTER 2 - (MATERIALS AND METHODS)

This section provides information for: i) harvesting rat ACL tissues, ii) performing mechanical testson the rat ACL tissue, iii) fabricating nanofiber scaffolds with an electrospinning device, and iv) characterization of the fabricated scaffolds in terms of diameter as well as tensile biomechanical properties. The experimental design, as well as the processes for harvesting and characterization are depicted in Figure 1 below.

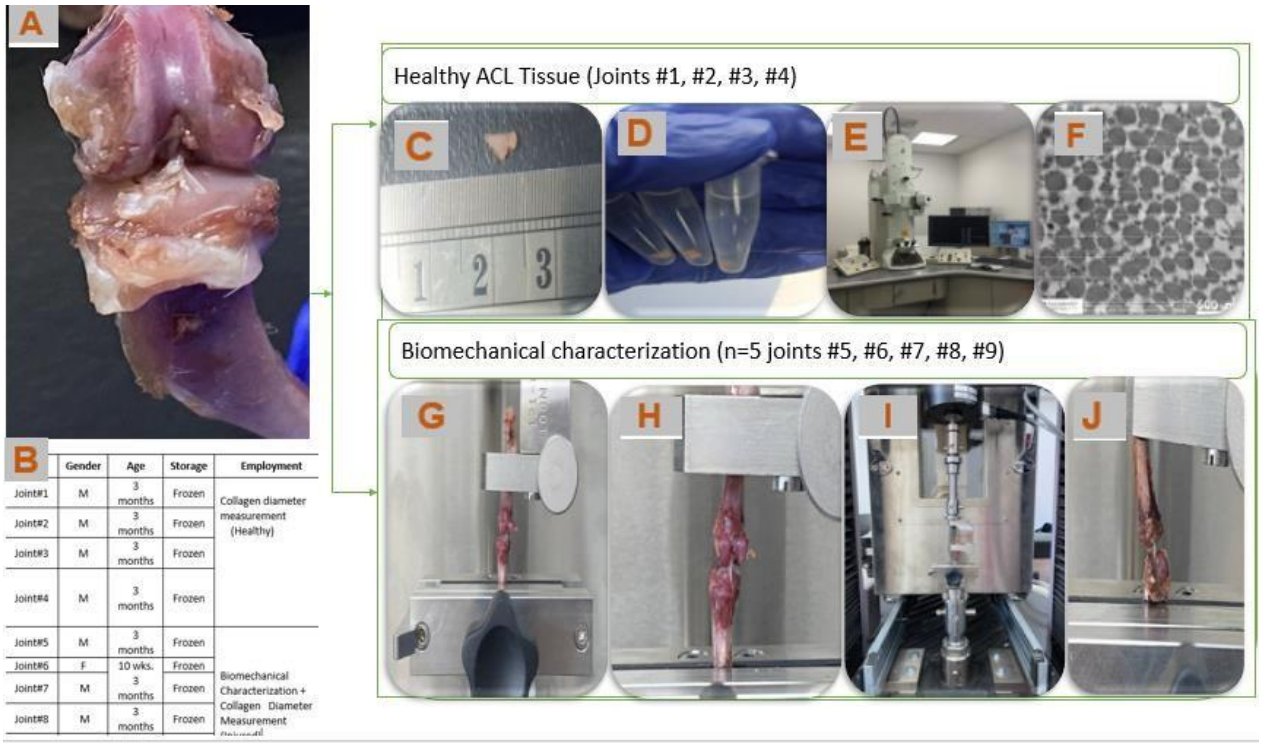

Figure 1: Native ACL harvesting and characterization

2.1 Materials

All chemicals were acquired from Sigma Aldrich, and their product numbers are listed below. Glutaraldehyde (Sigma Aldrich, #G5882), osmium tetroxide (1%, Sigma Aldrich, #75633), Phosphate buffer solution (Sigma Aldrich, #P5244), ethanol (Sigma Aldrich, #E7023), propylene oxide (Sigma Aldrich, #82320), epoxy embedding medium 812 substitute (Sigma Aldrich, #45345), polycaprolactone (Sigma-Aldrich, #440744), dichloromethane (Sigma Aldrich, #270997), N-N-Dimethylformamide (Sigma Aldrich, #319937), epoxy embedding medium hardener DDSA (Sigma Aldrich, #45346), epoxy embedding medium hardener MNA (Sigma Aldrich, #45347), epoxy embedding medium accelerator DMP 30 (Sigma Aldrich, #45348), Polycaprolactone (Sigma-Aldrich, ##440744), acetic acid (#270725), formic acid (90%, #110854), pyridine (Sigma-Aldrich #270970).

2.2 Harvesting the ACL Tissue

The rat limbs were picked up from the National Biotechnology Center (Nur-Sultan, KZ) shortly after the animals were slaughtered (Figure 1B, n=9) and preserved at -20^{o}C until needed. Before testing, the frozen knee joints were thawed at room temperature. A surgical blade was used to remove all tendons and ligaments from the joint except the ACL (Figure 1A).

2.3 Biomechanical Tests

A uniaxial material testing machine with a 1 kN load cell (MTS Criterion Model 43, MTS Systems Co., Eden Prairie, MN, USA) was used to assess the biomechanical parameters of ACL tissues. A custom-made jaw assembly was used to mount the Tibia-ACL-Femur joint to the unit, and the ACL's

axis was aligned with the load axis of the testing equipment. An initial load of 0.3N was applied to straighten the specimens (Figure 1G) and the specimens were stretched till failure at a continuous crosshead speed of 5 mm/min (Figure 1H-J). Biomechanical characteristics were tested on a total of five joints (n=5). Upon reaching the state of failure, the knee joints were removed, and the ruptured ACL was used to represent the injured ACL tissue, and all five specimens were employed in fibril diameter measurements to portray diameter distribution of injured ACL tissue. This ex-vivo ACL injury model was previously applied successfully [32].

2.4 Preparing Rat ACL for TEM Characterization

The diameter and distribution of collagen fibrils were measured using Transmission Electron Microscopy (TEM) images of tissue sections. First, the ACL tissue was located, it was stretched for better visibility, and it was removed from the joint to provide a specimen with dimensions of approximately 2mmx2mmx2mm from the middle section of the tissue (Figure 1C, n=4). To prepare injured ACL tissue, after rupture of the ACL tissues, a representative specimen with the size of 2mmx2mmx2mm was recovered from the injured ACL tissues from the region close to the point of rupture (n=5). TEM characterization was performed on the middle region of the tissue specimen.

To prepare the TEM specimens, a method reported elsewhere was employed[32]. Briefly, first, the specimens were preserved with a 2.5 percent glutaraldehyde solution to prevent any possible modification in the joint structure during processing (Figure 1D). The specimens were then held at ambient temperature for fixation and then gradually cooled down to 4°C. To slow down autolytic processes and minimize tissue shrinking, this form of cooling is required. Phosphate buffer solution (PBS) was used to wash the specimens three times for ten minutes each time. A subsequent fixation with 1 percent osmium tetroxide for 2 hours was used to give the specimen additional stability.

Osmium tetroxide was employed as both a fixative and a contrasting substance. Specimens were washed twice in PBS for 10 minutes each time after fixation. As a transitional solvent, the specimens were dehydrated using a graded series of 50 percent ethanol for 40 minutes, 70 percent ethanol for 12 hours, 96 percent ethanol for 20 minutes twice, 100 percent ethanol for 15 minutes twice, and a mixture of 100 percent ethanol and propylene oxide for 10 minutes. To ensure a seamless transition, a graded ethanol sequence was used to prevent any alterations in tissue structure. After that, different resin and propylene oxide combinations were used to penetrate the dried specimens. Various amounts of epoxy mix medium components 812, DDSA (Dodecenylsuccinic anhydride) and MNA (Methyl nadic anhydride) were used to make the resin. Infiltration was used to fill blocks of samples with resin to make them hard enough to bear pressure during sectioning and cutting. Samples were submerged in a 1:1 mixture of resin and propylene oxide for 2 hours at 37°C. After 2 hours at 37°C, the mixture was adjusted to a 3:1 ratio, followed by 12 hours of pure resin. Different resin and propylene oxide mixes were submerged in molds for 24 hours in the next step. The implanted samples were polymerized over the course of two days at 60°C.

Finally, using an ultra-microtome (Boeckeler PT-PC PowerTome Ultramicrotome, USA), a thin slice perpendicular to the longitudinal axis of the ligament was cut and utilized to complete the experiment. By pressing the block to the sides in regulated increments over a diamond knife, this one-of-a-kind piece of equipment may be used to cut specimen components. The chopped portions are collected and filled with distilled water on this piece of equipment. Each slice was selected to be roughly 60 nm in size. A Transmission Electron Microscope (JEOL JEM-1400Plus 120kV TEM) was utilized to capture high magnification pictures of ACL sections (Figure 1E,F). Perpendicular cuts of fibrils were optimized to obtain cross-sectional pictures representing specimens from various regions of the collected tissue. For each specimen, around ten slices were photographed. In this method, roughly 40 sections of healthy and injured ACL tissues were collected for each group.

2.5 Measurement of ACL Fibril Diameter

On the TEM images, 10 equally separated parallel lines were created, and the diameter of fibrils crossing these lines was measured. The diameter of each fibril was measured using the ImageJ image processing program (National Institutes of Health, US). The fibrils in each portion were counted toa minimum of 100 per section, with three sections utilized for each joint. Over 300 typical readingswere acquired for each of the two groups of ACL tissues, both in healthy and in injured condition.Finally, for each group, the diameter distribution, mean diameter, and ranges were calculated usingthe data (for healthy and injured ACL). SEM images of PCL scaffolds were used similarly to calculate the diameter of the fibers in the scaffolds.

2.6 Nanofiber Scaffold Fabrication

The scaffold was fabricated using polycaprolactone with a molecular weight of 80000 g/mol (Sigma-Aldrich, ##440744). PCL solutions in different concentrations were produced in preparation for the electrospinning procedure. Bimodal and unimodal distributions were obtained by dissolving PCL in an acetic acid (#270725) and formic acid (#110854) solution with pyridine to get a final volume of 1 mL (Table 1). The solutions were prepared by mixing the materials at 40°C for 2 hours while stirring constantly at 1500 rpm on a magnetic stirrer [Cat#US152D, Bibby Scientific].

A co-electrospinning process (Figure2) was utilized to fabricate aligned nanofibers with a bimodal distribution, which were then characterized. The concentrations of PCL were 8 percent and 15 percent, respectively. The solutions were poured into two syringes that were placed at a position facing one another and directed to the rotating drum collector. The voltage of the power supply was adjusted to 9 kV, and the drum revolved at a speed of 2000 revolutions per minute. A 7cm gap between

the spinneret and the drum collector was established. On a stationary plate, unaligned fibers were created at 9kV by feeding a 10 percent PCL solution at a flow rate of 0.03 ml/h (Figure 3).

Scaffold Type		Material Properties				Process Parameters				
		PCL (gr)	Acetic Acid (ml)	Formic Acid (ml)	Pyridine (ml)	Flow rate (ml/h)	Distance (cm)	Drum Speed (RPM)	Needle Diameter (G)	Voltage (kV)
Bimodal	8%	0.08	0.5	0.5	0.006	0.03	7	2000	21	9
	15%	0.15	0.5	0.5	0.02	0.06	7	2000	21	9
Unimodal	10%	0.10	0.5	0.5	0.006	0.03	7	2000	21	9

Table 1: Composition of the ingredients to prepare bimodal and unimodal scaffolds

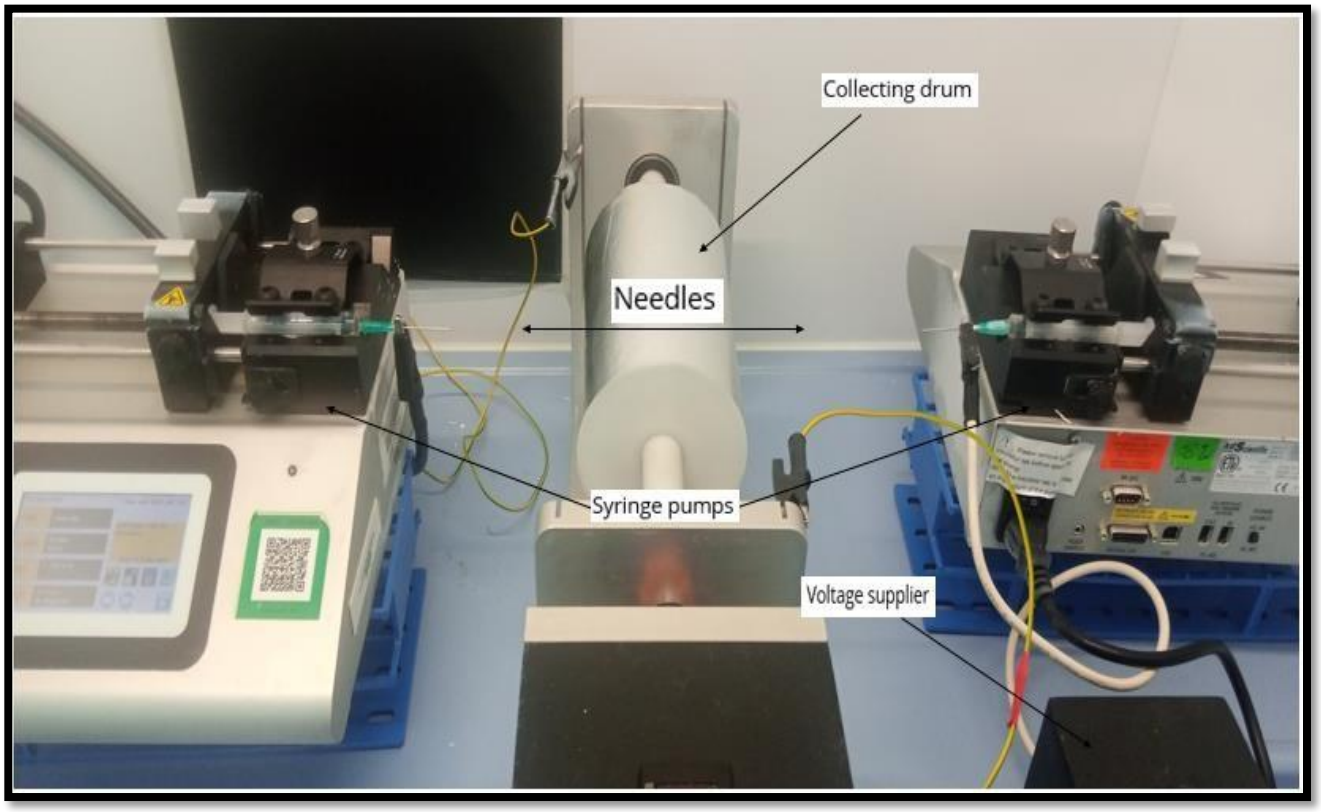

Figure 2: Setup for electrospinning scaffold fabrication in an aligned approach

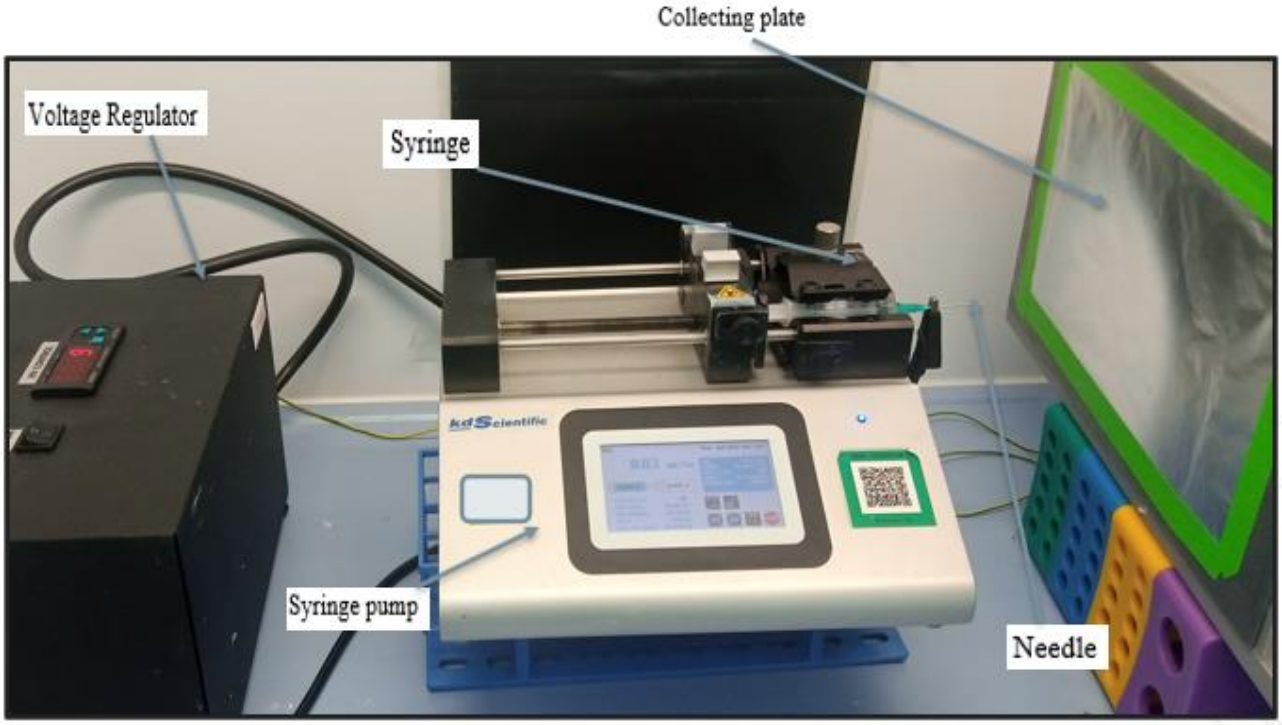

Figure 3: Unaligned random scaffold electrospinning setup

2.7 Mechanical Properties of PCL Scaffolds

The mechanical characteristics of PCL scaffolds were determined using uniaxial material testing equipment (MTS Criterion Model 43, MTS Systems Co., Eden Prairie, MN, USA) mounted with a one-kilogram load cell (Figure 4). The specimens were cut in dimensions of 5cmx1cm (length xwidth) and the thickness of the scaffold was measured using a digital caliper (Faithful Quality Tool, UK, Faicaldig digital caliper 150mm) by placing the specimen between two glass slides (Fig 4A). Tension was applied to PCL scaffolds (n=5 per group) using custom-made grips, and the scaffolds were strained with an initial 0.01N preloading (Fig 4B). The test was performed until failure at a crosshead speed of 5 mm/min (Fig 4C).

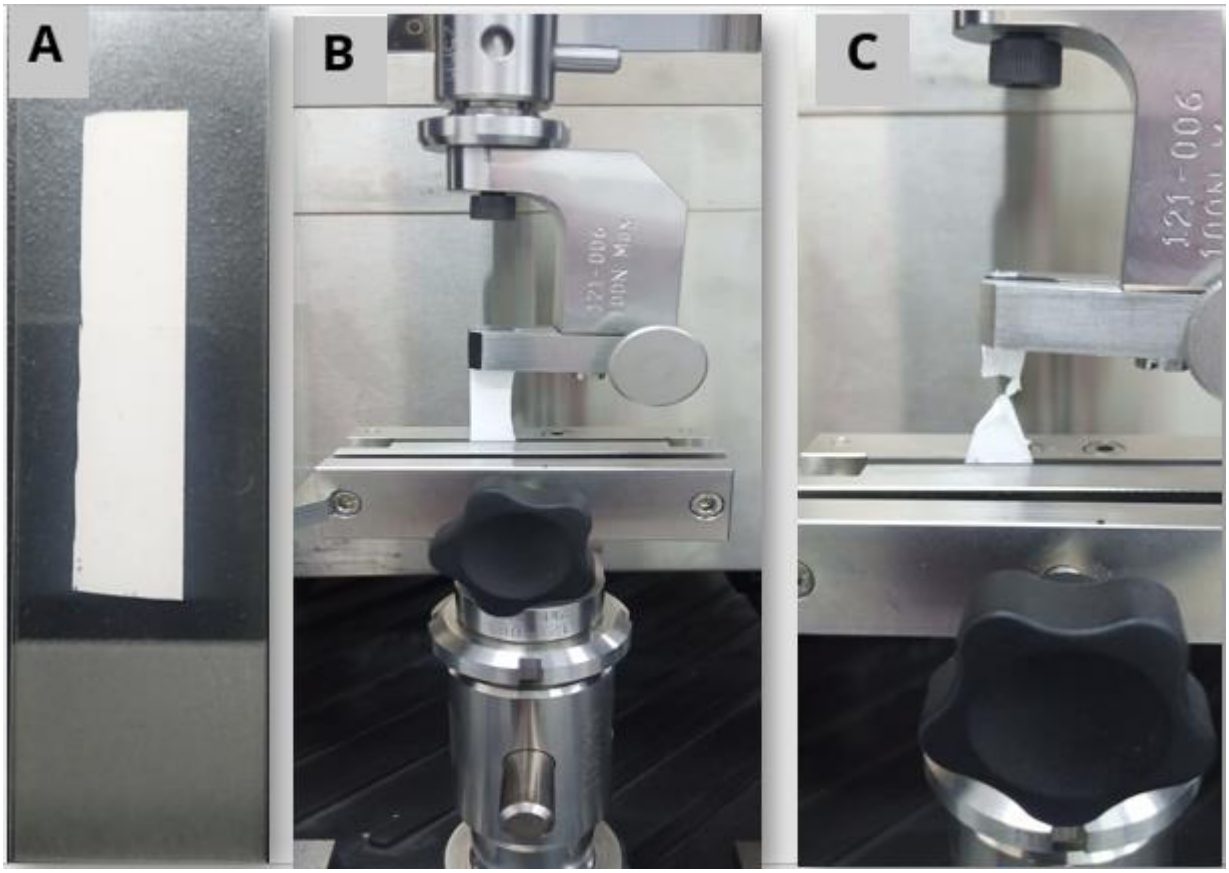

Figure 4: (A) 5cm x 1cm scaffold for thickness and width measurement, (B) Fixed scaffold on the mechanical testing device, and (C) scaffold ruptured at the midsection

2.8 Scanning Electron Microscopy Characterization

A turbo-pumped sputter coater (Quorum Q150T ES, UK) was used to coat the specimens with a 5nm thickness of gold layer at a current of 20mA. The scaffolds were examined at different magnifications using a Scanning Electron Microscope (JSM- IT200(LA), JEOL, Japan). The diameters of scaffold fibers were measured using ImageJ (National Institute of Health, USA) software. The fiber diameter distribution of unaligned scaffolds and aligned bimodal scaffolds was measured using at least 150 fibers per picture (n=5 image/group) following a similar method described in Section 2.5.

2.9 Statistical Analysis

The mechanical parameters of the aligned (bimodal) and unaligned (unimodal) scaffolds were compared to the mechanical properties of normal Rat ACL tissue using One-Way analysis of variance (ANOVA) with Tukey HSD (Honestly Significant Difference) post-hoc test. The fibril diameters of healthy and injured ACL tissues, the diameters of aligned and unaligned scaffold fibers as well as those of collagen fibrils and scaffold fibers were compared using a t-test. The difference was considered significant when the p-value was less than 0.05 ($p<0.05$).

Chapter 3 – (RESULTS)

3.1 Diameter of Collagen Fibrils

The frequency distributions of collagen fibril diameter of healthy and injured ACL tissue are shown in Figure 5A and 5B, respectively. TEM photos of the corresponding histograms are also shown. The healthy ACL tissue appears to have a bimodal distribution, while the injured ACL tissue has a unimodal distribution. In addition, the healthy specimens showed a well-organized morphology, with collagen fibrils that were aligned in the longitudinal direction of the specimens(Fig. 5 A1, A2, A3) as determined by the roundness of the circles. Collagen fibrils structures generally have a circular shape. However, TEM images of injured specimens demonstrate a disorganized structure as shown by fibrils aligned in diverse orientations on the specimens' surfaces (Figure 5 B1, B2, B3).

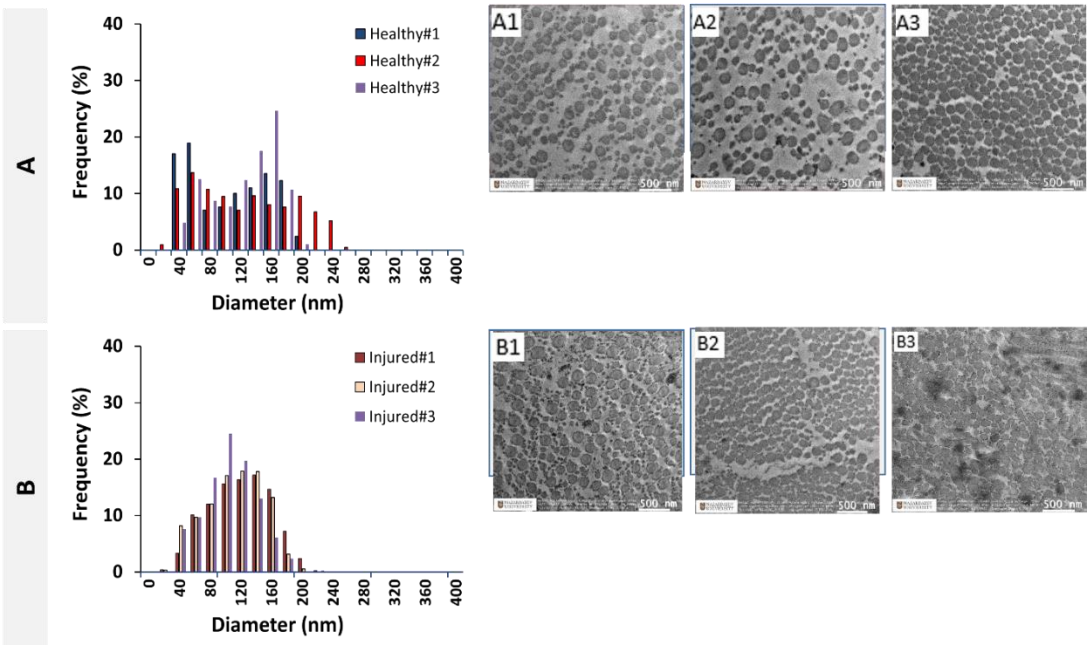

Figure 5: Healthy (A) and injured (B) diameter distribution of native ACL collagen fibrils and TEM images (Healthy: A1-A3, Injured: B1-B3).

Figure 6 shows the combined distributions of ACL fibrils from injured and healthy ACLs. ACL tissue from the injured knee demonstrated a unimodal distribution with one peak at 127 ± 11.5 nm,while the healthy tissue showed a bimodal (two peaks) distribution with peaks at 60 nm and 153±11.5 nm. A reduction in the diameter range of fibrils was observed from 20-260nm to 20-220nm, with the mean number average diameter value decreasing from 119.6 ±13.7 to 111.0 ±7.61 nm (Fig. 6C). The mean diameter also decreased, going from 110.2 ± 10.8 nm to 105.0 ± 6.28 nm. Generally speaking, the diameter distribution of collagen fibrils in the rat ACL changed from a bimodal to a unimodal distribution after the injury, demonstrating a decrease in average diameters ($p>0.05$). None of these changes was found to be statistically significant.

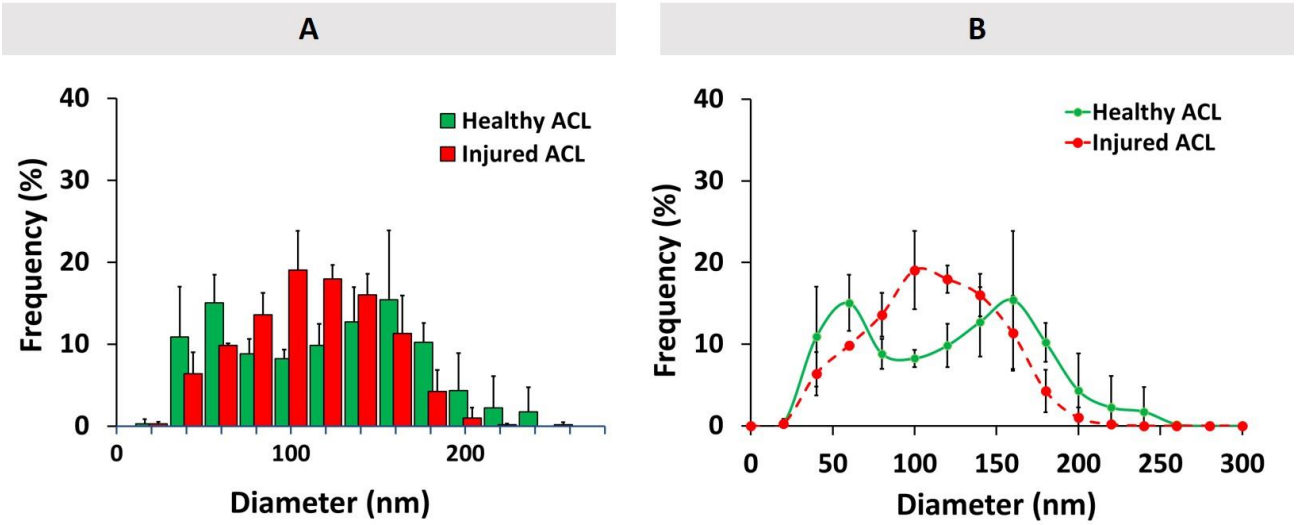

C

Fibril Diameter (nm)	Healthy ACL		Injured ACL
Range	20-260		20-220
Peak(s)	60±0.0	153±11.5	127±11.5
Mean Diameter	110.2±10.8		105.0±6.28
Number Average Diameter	119.6±13.7		111.0±7.61

*** p<0.05**

Figure 6: Healthy and Injured ACL diameter distributions in the histogram (A) and line graph (B). Error bars show standard deviation (n=4).

3.2 Fiber Diameter of PCL Scaffolds

The histograms of the aligned (bimodal) and unaligned (unimodal) PCL scaffolds are shown belowin Figure 7, along with the corresponding SEM images of the scaffolds. The aligned scaffolds exhibited a bimodal distribution (Figure 7A). The random scaffolds had a unimodal distribution (Figure 7B).

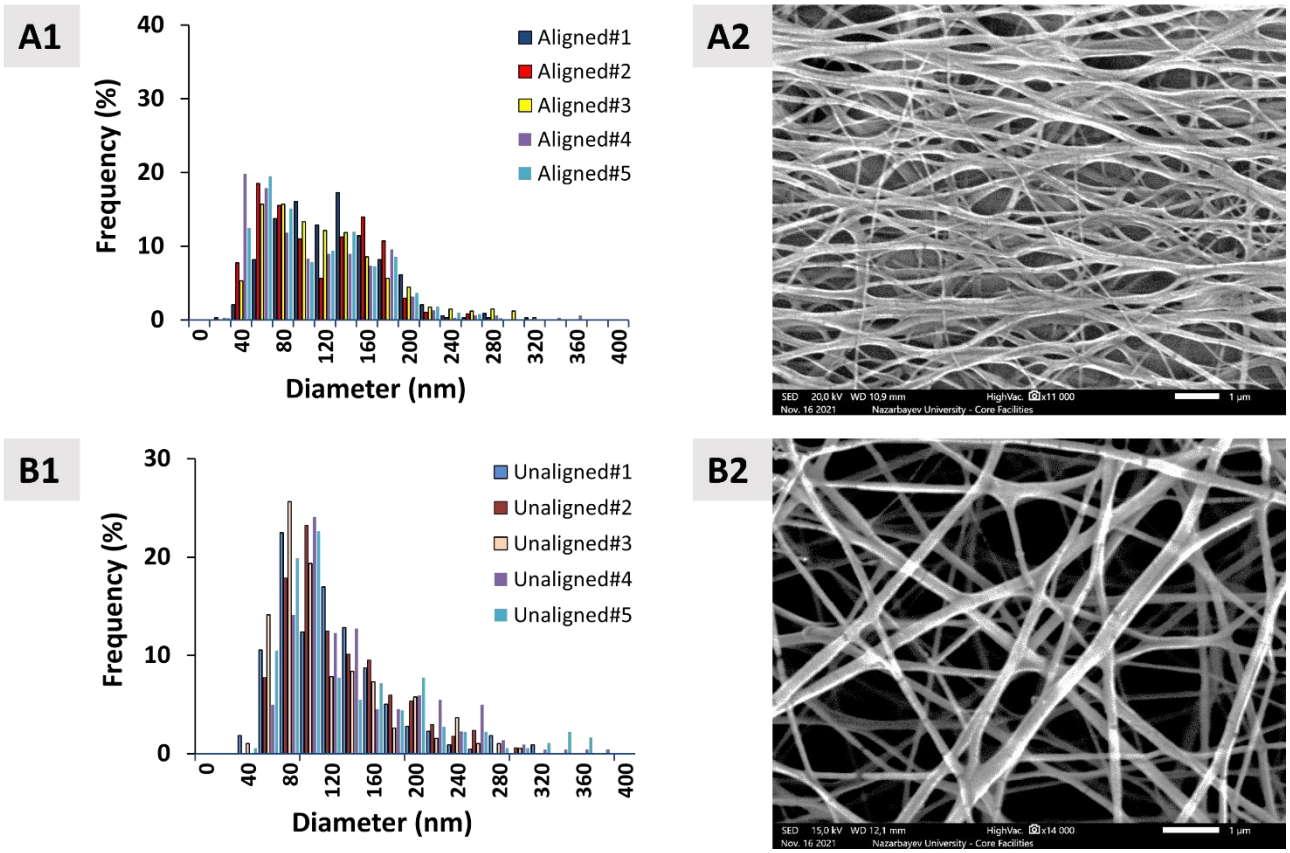

Figure 7: Diameter distribution of (A1) aligned and (B1) unaligned PCL fibers and corresponding representative SEM images (A2 and B2, n=5). Scale bar = 1μm.

Figure 8 below demonstrates the combined fiber diameter distribution for PCL scaffolds that are aligned and those that are not aligned. Results show that there is no statistically significant difference between the diameters of aligned and unaligned scaffolds in terms of mean diameter and number average diameter.

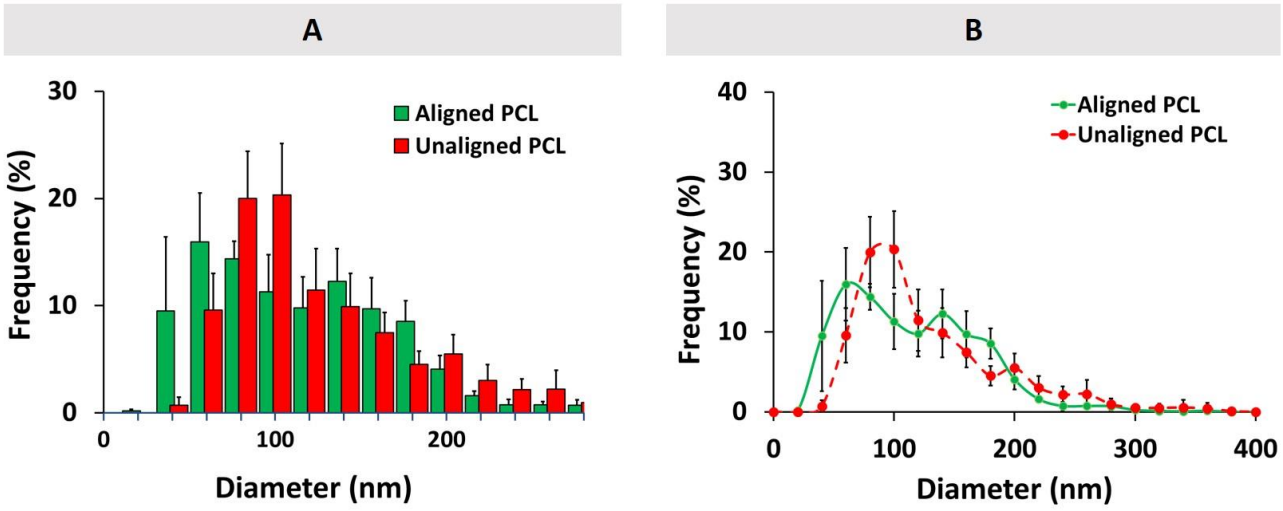

C

Fibril Diameter (nm)	Aligned Scaffold		Unaligned Scaffold
Range	20-360		40-380
Peak(s)	66±22	155±19	92±11
Mean Diameter	106±8.7		119±10
Number Average Diameter	115±9		128±9.9

* p<0.05

Figure 8: Combined aligned and unaligned PCL fiber diameter distributions in the form of (A) histogram and (B) line graph (n=4). Error bars denote standard deviation.

Comparison of ACL collagen fibril diameters and PCL scaffold fiber diameters are given in Figure 9. No statistically significant difference was observed between the diameters of aligned PCL fibers and healthy ACL fibrils ($p>0.05$). Unaligned PCL scaffold fiber diameters, on the other hand, were different from the injured ACL fibril diameters ($p<0.05$).

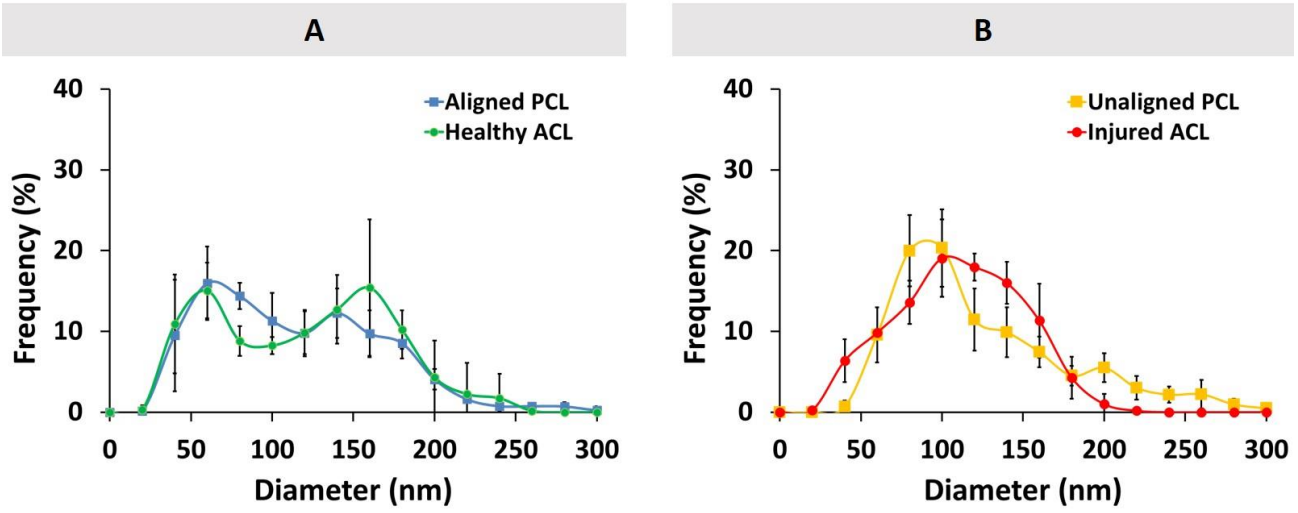

C

Fibril Diameter (nm)	Healthy ACL		Aligned Scaffold Bimodal		Injured ACL	Unaligned Scaffold Unimodal
Range	20-260		20-360		20-220	40-380
Peak(s)	60±0.0	153±11.5	66±22	155±19	127±11.5	92±11*
Mean Diameter	110.2±10.8		106±8.7		105.0±6.28	119±10*
Number Average Diameter	119.6±13.7		115±9		111.0±7.61	128±9.9*

* indicates difference between Healthy ACL and Aligned PCL or Injured ACL and Unaligned PCL at p<0.05

Figure 9: Comparison of diameter distribution between ACL tissue and PCL scaffolds. (A) Healthy ACL versus Aligned PCL, and (B) Injured ACL versus Unaligned PCL

Fiber alignment of aligned and unaligned PCL scaffolds in the form of mean angle are presented in Figure 10. As clearly seen from Figure 10, the aligned bimodal scaffolds contained fibers aligned longitudinally as depicted by a normal mean angle distribution (Figure 10.A1&C). Random unimodal scaffolds, on the other hand, depicted a flatter distribution of mean angle of fibers, indicating an obvious deviation from alignment (Figure 10.B1&C).

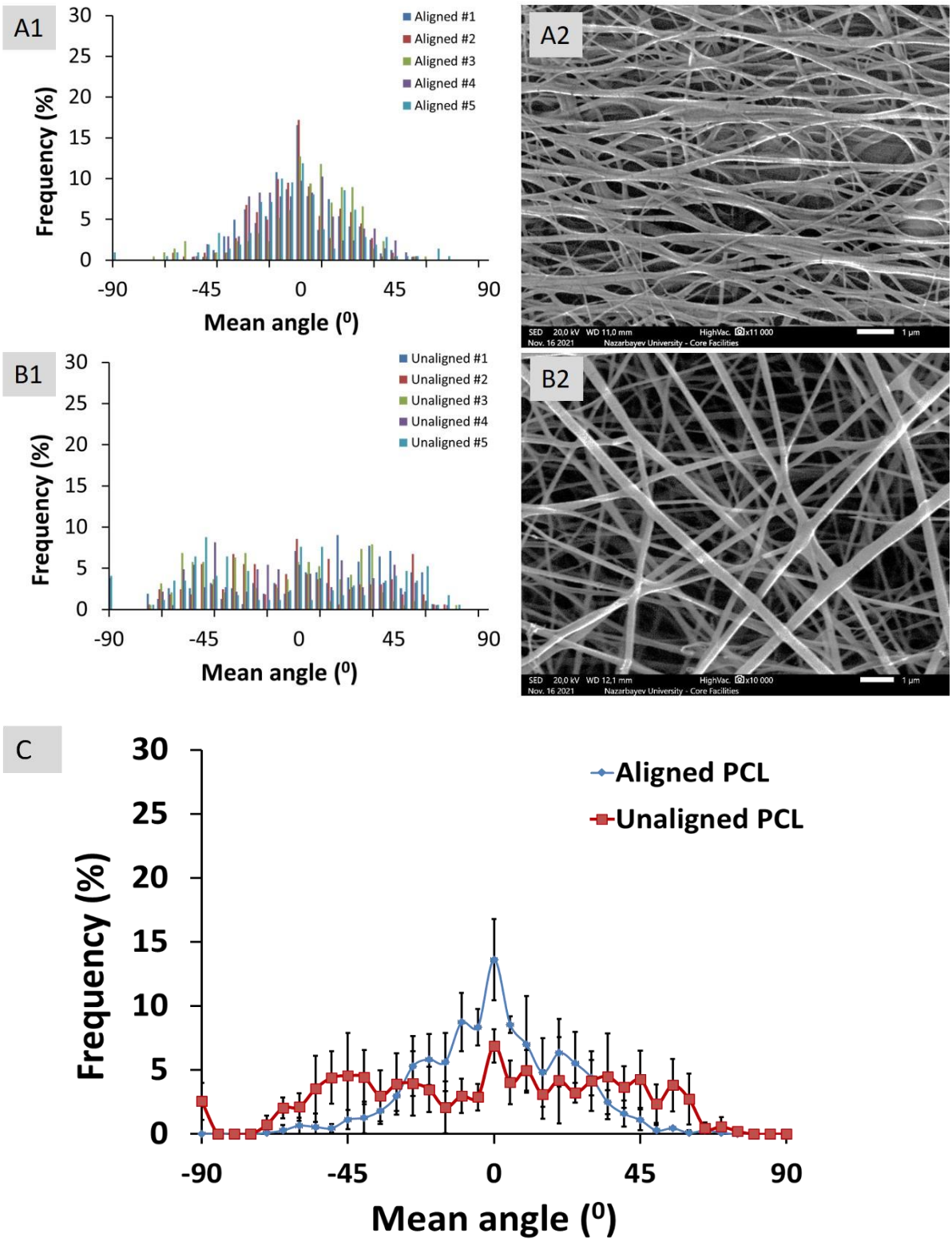

Figure 10: Fiber orientation distribution of (A1) Aligned and (B) Unaligned scaffolds (n=5), their representative SEM images (A2 and B2), and a line graph comparing the two scaffolds. Error bars represent standard deviation

3.3 Biomechanical Characterization of ACL Tissue and PCL Scaffolds

The load-elongation and stress-strain behavior of healthy ACL tissue are shown in Figure 11. It exhibits an initial toe area followed by a linear region and ends with a yield region. The ACL tissue has a tri-phase pattern that is typical. The ultimate stress and strain in the ACL tissue are 18.2 ± 3.9 MPa and 38.3 ± 17.4 percent, respectively. The tissue modulus was determined from the slope of the linear portion of the stress versus strain curve and is 0.64± 0.17 MPa for this particular specimen. The stiffness was found to be 17.6 ± 5.6 N/mm when the material was stressed. The ACL was stretched to an ultimate load of 17.1 ± 4.0 N with an elongation of 1.28 ± 0.44 mm.

The load-elongation and stress-strain curves for the PCL scaffolds are also shown in Figure 11. The tensile pattern of the PCL scaffolds was typical of tri-phasic tensile patterns, including toe, linear, and yield regions. The results for the typical mechanical performance parameters of PCLscaffolds are also shown in Figure 11C. The ultimate stress and strain of the aligned PCL scaffolds were determined to be 2.0 ± 0.8 MPa and 10.9 ± 1.1 percent, respectively, in the aligned PCL scaffolds. Similarly, the ultimate stress and strain of the unaligned PCL scaffolds, which represented the injured ACL tissue, were 2.6± 1.2 MPa and 22.5±1.4 percent, respectively. The moduli of the scaffolds with the aligned and unaligned organization were 0.22± 0.05 MPa and 0.17± 0.06 MPa, respectively, for the aligned and unaligned scaffolds. The stiffness of aligned and unaligned scaffolds was found to be 1.21 ± 0.30 N/mm and 0.77±0.12 N/mm, respectively, for the two categories of scaffolds. Employing aligned and unaligned scaffolds, the ultimate tensile load was 2.42±0.25 N and 2.40±0.24 N, respectively, when stretched to an ultimate elongation of 2.6±0.57 mm and 4.82± 0.71 mm, respectively.

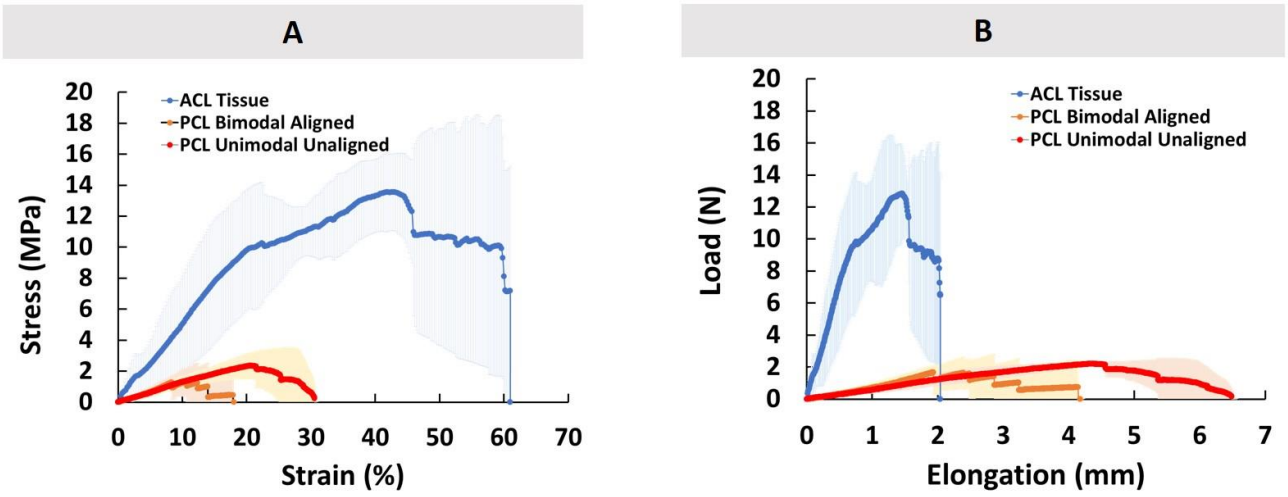

C	Ultimate Stress (MPa)	Ultimate Strain (%)	Strain at Break (%)	Modulus (MPa)	Stiffness (N/mm)	Ultimate Load (N)	Ultimate Strain (mm)
ACL	18.2±3.9$^{\#,*}$	38.3±17.4$^{\#}$	49.6±23.8$^{\#}$	0.64±0.17$^{\#,*}$	17.6±5.6$^{\#,*}$	17.1±4.0$^{\#,*}$	1.28±0.44$^{\#,*}$
PCL-Aligned	2.0 ± 0.8	10.9±1.1	11.1±1.0	0.22±0.05	1.21± 0.30	2.42 ±0.25	2.6 ±0.57*
PCL-Unaligned	2.6±1.2	22.5±1.4	28.2±2.3	0.17±0.06	0.77±0.12	2.40±0.24	4.82±0.71

Figure 11: Comparison of Native ACL tissue and PCL scaffold in terms of mechanical properties. (A) Stress-strain diagram, (B) Load-elongation diagram. (C) descriptive statistics. An * indicates significant difference from PCL-Aligned and # indicates significant difference from PCL-Aligned and # indicates significant difference from PCL-Unaligned at p<0.05. Error bars represent SD.

CHAPTER 4 - (DISCUSSION)

The distributions of collagen fibril diameter in rat ACL tissue before and after injury, as well as the tensile properties of healthy ACL tissue were investigated in this thesis. To establish the appropriateness of the PCL scaffolds for ACL repair/regeneration, the tensile properties as well as the fiber diameter distributions were also investigated. The rat ACL's collagen fibril diameter distribution shifted from bimodal to unimodal after rupture, with a reduction in the mean diameter of the collagen fibrils. The fiber diameter distributions of electrospun PCL scaffolds were designed to have a bimodal and unimodal appearance, enabling it to look qualitatively and quantitatively similar to healthy and injured ACL tissues. ACL collagen fibers are structured into fibril bundles that produce an orderly parallel wave pattern along the long axis of the collagen fibers, as seen in the TEM images. The mechanicalproperties of ACL are enhanced as a result of this hierarchical configuration[34]. Our findings demonstrated that the ACL tissue of a healthy rat has a well-organized/aligned pattern of collagen fibrils, which is altered when the tissue is injured. Similar to what is observed in the rat ACL tissue, a ruptured bovine [32], sheep [33] and human [35] ACL was found to have a disorganized collagen fibril pattern.

Previous studies on the bovine ACL revealed diameter peaks of around 100 and 250 nm before the injury, which then changed to a single peak of 100 nm after injury [32]. A similar alteration occurred in the collagen fibril diameter of human ACL, which had an average diameter of 75 nm (20-185 nm) before being reduced to 71 nm (20-290 nm). Also, previous studies on the sheep ACL showed diameter peaks of around 100 and 250 nm before the injury, which then changed to a single peak of 100 nm after injury[33]. The diameter distribution of collagen fibrils in the ACL of healthy and injured rats was investigated in this thesis study. The results revealed that the mean diameter of fibrils

reduced following mechanical deformation and this resulted in a changein the modality from bimodal to unimodal. Both the findings obtained by Beisbayeva *et al* [32] on bovine ACL tissue, Smatov *et al* [33] on sheep ACL tissue and our results obtained on rat ACL tissue demonstrate similar behavior in terms of the distribution of diameters. In these investigations, the mean peak fibril diameters of healthy bovine and sheep ACL tissue were 73.3 ± 11.5nm / 213 ± 11.5nm and 75.6 ± 8.5nm / 157.6 ± 3.8nm, respectively. The mean peak fibril diameters of rat ACL tissue were 60 ± 0.0 nm and 153 ± 11.5 nm.

The electrospinning technique was used to create PCL electrospun scaffolds that represented the healthy and injured states of rat ACL tissues. The distribution of collagen fibril diameter of healthy and injured ACLs was represented by the aligned and unaligned PCL scaffolds, respectively. ACL collagen fibrils in both the healthy and injured states were seen to be both quantitatively and qualitatively imitated by PCLscaffolds with aligned structures. Unaligned scaffolds were unable to mimic the distribution of injured ACL tissue. Therefore, a fine tuning is needed in the composition of PCL solution to fabricate unimodal scaffolds. Even though the electrospinning approach is an excellent technique for the production of nanoscale scaffolds, producing fibers with controlled diameter requires tight control over the processing and material parameters [27].

There has been evidence that changes in the mean diameter and distribution of collagen fibrils in the ACL are important markers of tissue mechanics, and it has been shown that variations in fibril diameter, as well as distribution, have a direct influence on mechanical characteristics [4]. Bimodal distribution, such as seen in healthy ACL tissue, results in greater mechanical properties because the interfibrillar gaps between larger fibrils are filled with thinner fibrils to generate a densely packed ECM. This hierarchical structure of ligament tissue is altered, reducing the ligament tissue's capacity to withstand physiological stresses, and making the tissue mechanically more sensitive to injury. It should be highlighted that the mechanical parameters of healthy ACL tissue were the only ones

investigated in this research. Due to lack insufficiency of tools to measure the mechanical properties of the injured ACL tissue, it has not been possible to compare the mechanical properties of injured ACL with the healthy ACL and the PCL scaffolds.

Each of the parameters examined in this research, including ultimate strain, ultimate stress, stiffness, and modulus, showed that the native ACL tissue outperformed both aligned and unaligned PCL scaffolds. A comparison of the two groups of scaffolds showed that the aligned and unaligned PCL scaffolds were similar in terms of all the parameters tested except ultimate strain.

This research study has certain methodological limitations, which should be noted. For example, owing to a lack of proper equipment, it was not possible to examine the mechanical features of an injured ACL. A measurement of this kind would allow for the comparison of unaligned PCL scaffolds and injured ACL tissue, for example. The mechanical characteristics of ACL tissue were also studied in this work by applying tensile stress to the Femur Anterior Tibial Cruciate, even though biomechanical stress in the sagittal plane is the most common cause of ACL injury[38].

CHAPTER 5 - (CONCLUSION)

This study investigated the morphological and mechanical features of the native rat ACL tissue before and after injury. The collagen fibril diameter distribution shifted from bimodal to unimodal when the rat ACL ruptured, with a subsequent decrease in the average fibril diameter. The fiber diameter distributions of bimodal PCL scaffolds both quantitatively and qualitatively matched the collagen fibril diameter distribution of healthy ACL tissue, accompanied with significantly lower mechanical properties. To the best of our knowledge, there is currently no published research on the utilization of nanofiber-based scaffolds with bimodal distribution for ACL reconstruction/regeneration. This bimodal scaffold that is designed and fabricated here could be utilized as a synthetic graft in ACL reconstruction, and is expected to have significant impact on the improvement of orthopedic related research.

REFERENCE LIST

[1] V. B. Duthon, C. Barea, S. Abrassart, J. H. Fasel, D. Fritschy, and J. Ménétrey, "Anatomy of the anterior cruciate ligament," *Knee Surgery, Sport. Traumatol. Arthrosc.*, vol. 14, no. 3, pp. 204–213, 2006.

[2] W. Petersen and B. Tillmann, "Anatomie und funktion des vorderen kreuzbandes," *Orthopade*, vol. 31, no. 8, pp. 710–718, 2002.

[3] W. Petersen and T. Zantop, "Anatomy of the anterior cruciate ligament with regard to its two bundles," *Clin. Orthop. Relat. Res.*, no. 454, pp. 35–47, 2007.

[4] M. Marieswaran, I. Jain, B. Garg, V. Sharma, and D. Kalyanasundaram, "A review on biomechanics of anterior cruciate ligament and materials for reconstruction," *Appl. Bionics Biomech.*, vol. 2018, 2018.

[5] Y. Takeda, J. W. Xerogeanes, G. A. Livesay, F. H. Fu, and S. L. Y. Woo, "Biomechanical function of the human anterior cruciate ligament," *Arthroscopy*, vol. 10, no. 2, pp. 140–147, 1994.

[6] T. Zantop, W. Petersen, J. K. Sekiya, V. Musahl, and F. H. Fu, "Anterior cruciate ligament anatomy and function relating to anatomical reconstruction," *Knee Surgery, Sport. Traumatol. Arthrosc.*, vol. 14, no. 10, pp. 982–992, 2006.

[7] J. Zhu, X. Zhang, Y. Ma, C. Zhou, and yingfang Ao, "Ultrastructural and Morphological Characteristics of Human Anterior Cruciate Ligament and Hamstring Tendons," *Anat. Rec.*, vol. 295, no. 9, pp. 1430–1436, 2012.

[8] C. R. Allen, G. A. Livesay, E. K. Wong, and S. L. Y. Woo, "Injury and reconstruction of the anterior cruciate ligament and knee osteoarthritis," *Osteoarthr. Cartil.*, vol. 7, no. 1, pp. 110–121, 1999.

[9] N. A. Mall *et al.*, "Incidence and trends of anterior cruciate ligament reconstruction in the United States," *Am. J. Sports Med.*, vol. 42, no. 10, pp. 2363–2370, 2014.

[10] H. H. Lu and S. Thomopoulos, "Functional attachment of soft tissues to bone: Development, healing, and tissue engineering," *Annu. Rev. Biomed. Eng.*, vol. 15, pp. 201–226, 2013.

[11] K. Samuelsson, D. Andersson, and J. Karlsson, "Treatment of Anterior Cruciate Ligament Injuries With Special Reference to Graft Type and Surgical Technique: An Assessment of Randomized Controlled Trials," *Arthrosc. - J. Arthrosc. Relat. Surg.*, vol. 25, no. 10, pp. 1139–1174, 2009.

[12] B. D. Beynnon, R. J. Johnson, J. A. Abate, B. C. Fleming, and C. E. Nichols, "Treatment of anterior cruciate ligament injuries, Part 2," *Am. J. Sports Med.*, vol. 33, no. 11, pp. 1751–1767, 2005.

[13] R. Ma, X. Ju, X. H. Deng, and S. A. Rodeo, "A Novel Small Animal Model of Differential Anterior Cruciate Ligament Reconstruction Graft Strain," *J. Knee Surg.*, vol. 28, no. 6, pp. 489–495, 2015.

[14] G. Vunjak-Novakovic, G. Altman, R. Horan, and D. L. Kaplan, “Tissue engineering of ligaments,” *Annu. Rev. Biomed. Eng.*, vol. 6, pp. 131–156, 2004.

[15] V. S. Lin, M. C. Lee, S. O’Neal, J. McKean, and K. L. Paul Sung, “Ligament tissue engineering using synthetic biodegradable fiber scaffolds,” *Tissue Eng.*, vol. 5, no. 5, pp. 443–451, 1999.

[16] F. Akter, *Principles of Tissue Engineering*. Elsevier Inc., 2016.

[17] R. Kuroda, M. Kurosaka, S. Yoshiya, and K. Mizuno, “Localization of growth factors in the reconstructed anterior cruciate ligament: Immunohistological study in dogs,” *Knee Surgery, Sport. Traumatol. Arthrosc.*, vol. 8, no. 2, pp. 120–126, 2000.

[18] J. H. Brekke and J. M. Toth, “Principles of tissue engineering applied to programmable osteogenesis,” *J. Biomed. Mater. Res.*, vol. 43, no. 4, pp. 380–398, 1998.

[19] R. Vasita and D. S. Katti, “Nanofibers and their applications in tissue engineering,” *Int. J. Nanomedicine*, vol. 1, no. 1, pp. 15–30, 2006.

[20] S. Han *et al.*, “3D Electrospun Nanofiber-Based Scaffolds: From Preparations and Properties to Tissue Regeneration Applications,” *Stem Cells Int.*, vol. 2021, 2021.

[21] N. Ashammakhi, A. Ndreu, Y. Yang, H. Ylikauppila, and L. Nikkola, “Nanofiber-based scaffolds for tissue engineering,” *Eur. J. Plast. Surg.*, vol. 35, no. 2, pp. 135–149, 2012.

[22] S. C. Scherping, C. C. Schmidt, H. I. Georgescu, C. K. Kwoh, C. H. Evans, and S. L. Y. Woo, “Effect of growth factors on the proliferation of ligament fibroblasts from skeletally mature rabbits,” *Connect. Tissue Res.*, vol. 36, no. 1, pp. 1–8, 1997.

[23] M. M. Murray, K. Rice, R. J. Wright, and M. Spector, “The effect of selected growth factors on human anterior cruciate ligament cell interactions with a three-dimensional collagen-GAG scaffold,” *J. Orthop. Res.*, vol. 21, no. 2, pp. 238–244, 2003.

[24] T. Subbiah, G. S. Bhat, R. W. Tock, S. Parameswaran, and S. S. Ramkumar, “Electrospinning of nanofibers,” *J. Appl. Polym. Sci.*, vol. 96, no. 2, pp. 557–569, 2005.

[25] V. Beachley and X. Wen, “Effect of electrospinning parameters on the nanofiber diameter and length,” *Mater. Sci. Eng. C*, vol. 29, no. 3, pp. 663–668, 2009.

[26] N. Bhardwaj and S. C. Kundu, “Electrospinning: A fascinating fiber fabrication technique,” *Biotechnol. Adv.*, vol. 28, no. 3, pp. 325–347, 2010.

[27] C. Erisken, X. Zhang, K. L. Moffat, W. N. Levine, and H. H. Lu, “Scaffold fiber diameter regulates human tendon fibroblast growth and differentiation,” *Tissue Eng. - Part A*, vol. 19, no. 3–4, 2013.

[28] Y. Zhang *et al.*, “Efficient preparation of polymer nanofibers by needle roller electrospinning with low threshold voltage,” *Polym. Eng. Sci.*, vol. 59, no. 4, pp. 745–751, 2019.

[29] D. Y. Yang, S. H. Park, J. W. Hong, and J. H. Shin, “Quantitatively controlled fabrication of uniaxially aligned nanofibrous scaffold for cell adhesion,” *J. Nanomater.*, vol. 2011, 2011.

[30] M. Griffin, Y. Premakumar, A. Seifalian, P. E. Butler, and M. Szarko, “Biomechanical characterization of human soft tissues using indentation and tensile testing,” *J. Vis. Exp.*, vol. 2016, no. 118, pp. 1–8, 2016.

[31] T. T. Tower, M. R. Neidert, and R. T. Tranquillo, “Fiber alignment imaging during mechanical testing of soft tissues,” *Ann. Biomed. Eng.*, vol. 30, no. 10, pp. 1221–1233, 2002.

[32] Z. Beisbayeva, A. Zhanbassynova, G. Kulzhanova, F. Mukasheva, and C. Erisken, “Change in collagen fibril diameter distribution of bovine anterior cruciate ligament upon injury can be mimicked in a nanostructured scaffold,” *Molecules*, vol. 26, no. 5, 2021.

[33] S. Smatov, “Polycaprolactone based nanofiber scaffolds can mimic collagen fibril diameter distribution of healthy and injured sheep Anterior Cruciate Ligament,” 2021.

[34] T. Muellner *et al.*, “Light and electron microscopic study of stress-shielding effects on rat patellar tendon,” *Arch. Orthop. Trauma Surg.*, vol. 121, no. 10, pp. 561–565, 2001.

[35] J. Hashemi, N. Chandrashekar, H. Mansouri, J. R. Slauterbeck, and D. M. Hardy, “The human anterior cruciate ligament: Sex differences in ultrastructure and correlation with biomechanical properties,” *J. Orthop. Res.*, vol. 26, no. 7, pp. 945–950, 2008.

[36] J. B. Lee *et al.*, “Modification of PLGA nanofibrous mats by electron beam irradiation for soft tissue regeneration,” *J. Nanomater.*, vol. 2015, 2015.

[37] S. L. Y. Woo, Y. Takakura, R. Liang, F. Jia, and D. K. Moon, “Treatment with bioscaffold enhances the the fibril morphology and the collagen composition of healing medial collateral ligament in rabbits,” *Tissue Eng.*, vol. 12, no. 1, pp. 159–166, 2006.

[38] B. Yu and W. E. Garrett, “Mechanisms of non-contact ACL injuries,” *Br. J. Sports Med.*, vol. 41, no. SUPPL. 1, 2007.